Supplementary Information

Graphene Quantum Dots-Mediated Anchoring of Highly Dispersed Bismuth Nanoparticles on Porous Graphene for Enhanced Electrocatalytic CO_2 Reduction to Formate

Yi Cheng[a,b], Ruizhe Yang[a,b], Lu Xia[c], Xiaoli Zhao*[d],Yuwei Tan[a,b], Ming Sun[a,b], Suming Li[a,b], Fei Li*[e] and Ming Huang*[a,b]

[a]*Institute of Fundamental and Frontier Sciences, University of Electronic Science and Technology of China, Chengdu 611731, China*

[b]*Yangtze Delta Region Institute (Huzhou), University of Electronic Science and Technology of China, Huzhou 313001, China*

[c]*ICFO–Institut de Ciències Fotòniques, The Barcelona Institute of Science and Technology, Barcelona 08860, Spain*

[d]*School of Materials Science and Engineering, Xihua University, Chengdu, 610039, China*

[e]*School of Materials and Energy, University of Electronic Science and Technology of China, Chengdu 611731, China*

Corresponding Authors

*Xiaoli Zhao (zhaoxl@mail.xhu.edu.cn),

*Fei Li (feili@uestc.edu.cn),

*Ming Huang (huangming@uestc.edu.cn)

Materials

Bismuth nitrate pentahydrate ($Bi(NO_3)_3 \cdot 5H_2O$), commercial Bismuth and magnesium hydrate ($Mg(OH)_2$) were purchased from Shanghai Aladdin Biochemical Technology Co.,Ltd. Hydrochloric acid (HCl) and nitric acid (HNO_3) were purchased from Sichuan Xilong Science Co.,Ltd. All chemicals were used without further purification. The deionized water (18.2 MΩ cm^{-1}) was produced using an ultra-pure purification system.

Synthesis of graphene quantum dots

As previously documented, the synthesis of graphene quantum dots (GQDs) involved the refluxing of carbon black powder (0.2 g) with a 6 M solution of nitric acid (50 mL) for 24 h. Following this, centrifugation at 5000 rpm for 10 minutes was performed to eliminate larger particles. The resulting solution was then subjected to heat drying, yielding reddish-brown powders that were subsequently resuspended in deionized (DI) water. The obtained suspension underwent further filtration through a 0.22 μm microporous membrane to eliminate insoluble carbon byproducts. Subsequently, purification was carried out using a dialysis bag with a molecular weight cutoff of 3000 Da for a duration of 3 days. Finally, the purified product was freeze-dried to yield dark brown GQDs. The overall yield of the as-prepared GQDs is approximately 60%.

Synthesis of porous graphene

Porous graphene (PG) was synthesized through a chemical vapor deposition (CVD) process involving the deposition of graphene onto a MgO template, followed by an etching procedure to eliminate the MgO template. In a typical protocol, magnesium hydrate powder was loaded into an alumina boat, which was then placed inside a clean quartz tube within the CVD system. The CVD system was gradually ramped up to 1030 °C over the course of 1 hour and maintained at this temperature for an additional hour. Subsequently, the argon (Ar) flow was ceased, and a mixed gas flow comprising C_2H_4 (50 sccm) and H_2 (30 sccm) was introduced into the system for 1.5 h to facilitate the growth of graphene, resulting in the formation of MgO@graphene. The MgO@graphene composite was then dispersed in a 3 M aqueous HCl solution and subjected to constant stirring on a hot plate at 80 °C for 24 hours to remove the MgO template. The resulting porous graphene material was collected through filtration, thoroughly washed with deionized water multiple times, and subsequently freeze-dried for further use.

Synthesis of Bi NPs@PG and Bi SPs@PG

Initially, 100 mg of Bi $(NO_3)_3$ was dissolved in 50 mL of deionized water to form a transparent solution. Subsequently, 30 mg of GQDs was added to the above solution with vigorous stirring. After 30 mins, 100 mg of PG was added and stirred for 60 mins. The resulting solution was immediately cooled with liquid nitrogen, subjected to freeze-drying, and heat-treated at 400 °C for 60 mins at a heating rate of 3 °C min^{-1} under a mixed

gas flow of N_2 and NH_3. After heat-treatment, the Bi NPs@PG was obtained. The synthesis of Bi SPs@PG was carried out using the same procedure, excluding the addition of GQDs.

Materials characterization

X-ray diffraction (XRD) patterns were obtained using an XRD-6100 X-ray powder diffractometer with Cu Kα radiation (λ = 1.5406 Å). X-ray photoelectron spectroscopy (XPS) was conducted with an ESCALAB250Xi X-ray photoelectron spectrometer to analyze the composition and chemical states of catalysts. Field-emission scanning electron microscopy (FESEM; ZEISS MERLIN Compact) and transmission electron microscopy (TEM; JEOL JEM-F200) were conducted to characterize the microstructure of the synthesized catalysts.

Electrochemical characterization

Electrochemical tests were conducted using an electrochemical workstation (CHI 760E) in a customized gas tight H-type glass cell with the catalyst on glassy carbon as the working electrode, a platinum plate (1.5 cm × 1.5 cm) as the counter electrode, and Ag/AgCl electrode (3 M KCl) as the reference electrode in 0.1 M $KHCO_3$ electrolyte. A cation exchange membrane (Nafion 117) was used as the compartment separator. For working electrode, 10 mg catalyst was dispersed in the solution of 950 μL isopropyl alcohol and 50 uL Nafion (5%, D520, Dupont) and sonicated for 30 min to form a homogeneous ink. 30 uL of the ink was applied onto a 0.5 × 0.5 cm^2 carbon paper (Toray TGP-H-060) and dried at 40 °C for 4 h. Before the test, the electrolyte in cathode compartment was degassed by bubbling high-purity CO_2 for more than 30 mins under constant magnetic stirring (800 rpm) and was maintained in a CO_2-saturated state throughout the entire testing process, with a flow rate of 30 mL min^{-1} controlled by a mass flow controller. For flow cell test, 1 mg of the catalyst was applied onto a gas diffusion electrode (1.0 × 1.0 cm^2) as the cathode and Ti/IrO_2 was used as the anode. During the CO_2RR, 0.5 M $KHCO_3$ was used as electrolyte and circulated around both the anode and cathode at a flow rate of 6.2 mL min^{-1} during the CO2RR. High-purity CO_2 was passed through the gas chamber at a flow rate of 15 mL min^{-1}. The catalyst was pre-treated at -1.3 V (vs. Ag/AgCl) for 10 mins. Electrochemical impedance spectroscopy (EIS) was performed in a frequency range from 0.1 Hz to 100 kHz to determine the ohmic resistance (Rs). Linear sweep voltammetry (LSV) measurements were conducted from −0.2 V to −1.4 V vs. RHE at 5 mV s^{-1}. All the potentials were calibrated with reference to reversible hydrogen electrode (RHE) using the equation $E_{RHE} = E_{Ag/AgCl} + 0.21\ V + 0.0591\ V \times pH - R_s \times i$, where i was the average current. The pH of CO_2 saturated 0.1 M $KHCO_3$ electrolyte and 0.5 M $KHCO_3$ electrolyte were measured to be 6.8 and 7.2, respectively. Gaseous products generated during CO_2RR were transferred into a gas chromatograph (GC) equipped with both a flame ionization detector (FID) and a thermal conductivity detector (TCD) for online analysis. High-purity N_2 and H_2 were employed as carrier gases. Faradaic efficiencies (FE) for gaseous products (such as CO, CH_4, C_2H_4, H_2) were calculated using the following equations[1]:

$$FE = {}^{j_i}\!/_{j_{tot}} \times 100\% \quad (1)$$

$$j_t = x_i \times v \times \frac{n_i F P_0}{RT} \times \left(S_{electrode\ area}\right)^{-1} \quad (2)$$

$$j_{tot} = i \times \left(S_{electrode\ area}\right)^{-1} \quad (3)$$

Here, i is the recorded current, j_i is partial current density of the gas product and j_{tot} is the total current density. x_i denotes the volume fraction of the gas product as measured by GC, v represents the flow rate of CO_2, n_i is the number of electrons required to generate the product molecule, P_0 is the standard atmospheric pressure (101.325 kPa), F is Faradaic constant (96485.3 C mol^{-1}), R is the gas constant (8.314 J mol^{-1} K^{-1}), and T is room temperature (298.15 K).

Liquid products (mainly formate) were analyzed by ion chromatography (IC). Since the production of one formate molecule consumes two electrons, the Faradaic efficiency for formate is calculated as follows:

$$FE = \frac{2 \times 98458 \times C \times V}{Q} \times 100\% \quad (4)$$

where C is the concentration of formate, V is the injection volume to IC, and Q represents the quantity of electric charge.

In situ attenuated total reflectance surface-enhanced infrared absorption spectroscopy (ATR-SEIRAS) investigation

The electrochemical operando ATR-SEIRAS measurements were conducted using a Fourier-transform infrared spectroscopy (FTIR) spectrometer equipped with a mercury–cadmium–telluride (MCT) detector. To facilitate the surface-enhanced effect, Au films were chemically deposited on the reflective surface of a Si crystal, serving as the conductive substrate. The working electrode was prepared by drop-casting the sample onto the Au-deposited Si crystal, which was then integrated into a custom-made spectroelectrochemical cell attached to the ATR accessory. An Ag/AgCl electrode was employed as the reference electrode and a Pt foil was used as the counter electrode. During spectrum collection, the optical path was continuously purged with nitrogen gas to minimize the interference from water and CO_2 in the air. The electrolyte was CO_2-saturated 0.1 M $KHCO_3$ solution. Background measurement was taken at open circuit potential, and subsequent spectra were recorded at different potentials. All collected spectra were presented in terms of absorbance (-log(R/R0)), with a negative peak indicating the consumption of a specific substance or functional group and a positive peak indicating the production or increase of a particular substance or functional group.

Density functional theory (DFT) calculations

DFT calculations were performed using the generalized gradient correlation function within the Vienna Ab initio Simulation Package (VASP 5.4)[2-4]. The projector-augmented wave method was employed to model the electron-

ion interactions. A cut-off energy of 450 eV was applied, and a Gaussian smearing width of 0.2 eV was used[5, 6]. For structure optimization and electron-related features, a Monkhorst-Pack grid with a 3 × 3 × 1 k-point sampling in the Brillouin zone was used. A vacuum space of 15 Å was used for all calculations. All atoms (except the boundary atoms) were considered relaxed when the residual force was less than 0.01 eV $Å^{-1}$. The adsorption energy (E_{ads}) of reactants or reaction intermediates was calculated as follows:

$$E_{ads} = E_{tot} - (E_{mol} + E_{cat})$$

where E_{tot} represents the total energy of the adsorption system, E_{mol} denotes the energy of adsorbates, and E_{cat} stands for the energy of the catalyst, respectively.

The Gibbs free energy of each species was calculated as follows:

$$G = E_{DFT} + E_{ZPE} + \int C_p dT - TS$$

where E_{DFT} is the electronic energy directly obtained from DFT calculations, E_{ZPE} is the zero-point vibrational energy, C_p is the heat capacity, T is the room temperature (298.15 K), and S is the entropy.

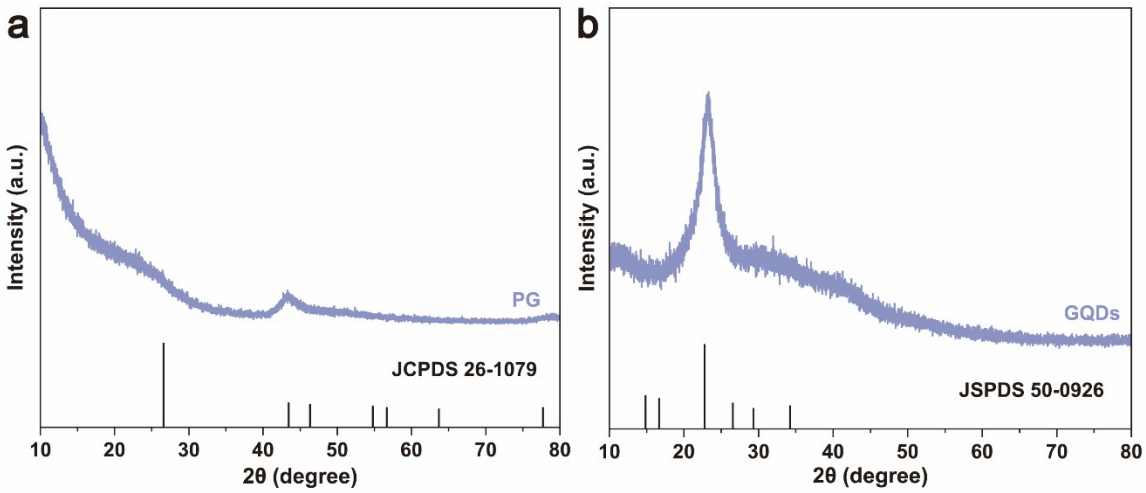

Fig. S1 XRD patterns of (a) PG and (b) GQDs.

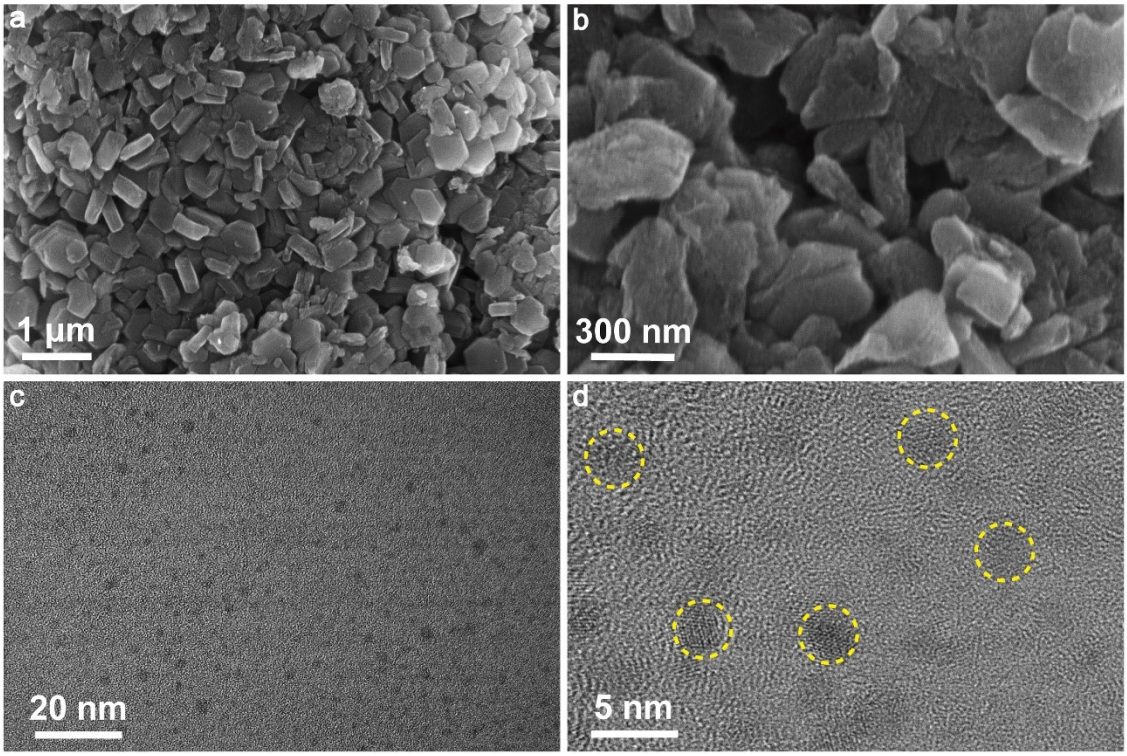

Fig. S2 (a, b) SEM images of PG, and (c, d) TEM images of GQDs.

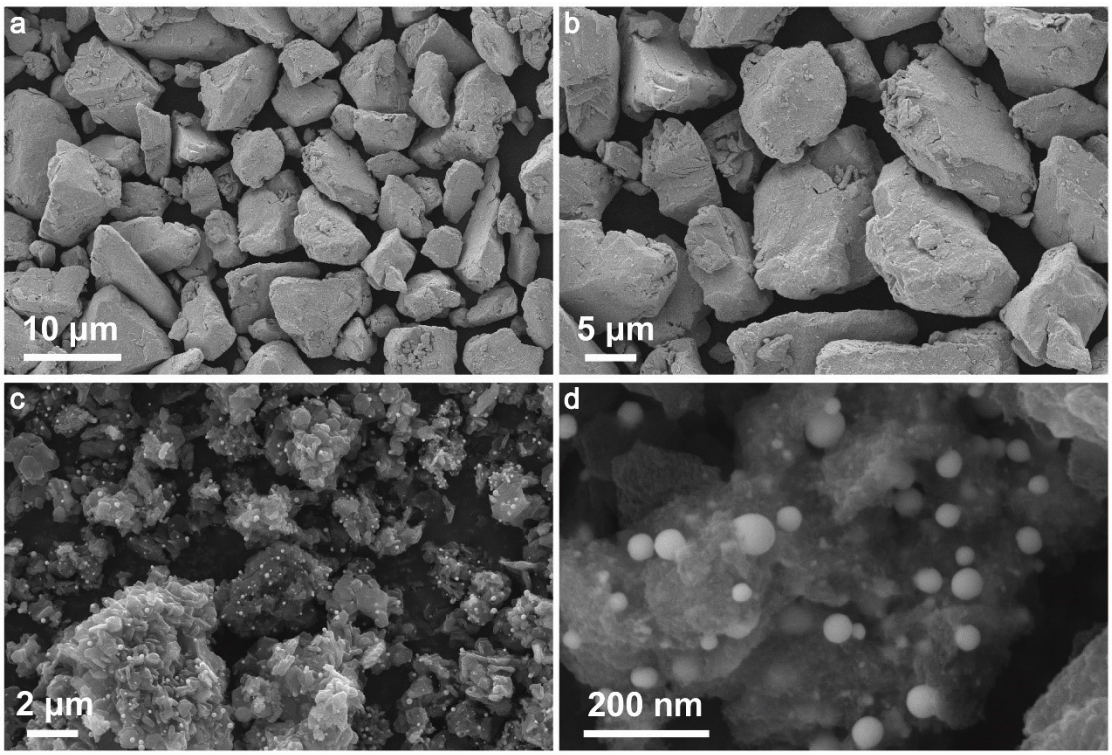

Fig. S3 SEM images of (a, b) commercial Bi and (c, d) Bi SPs@PG.

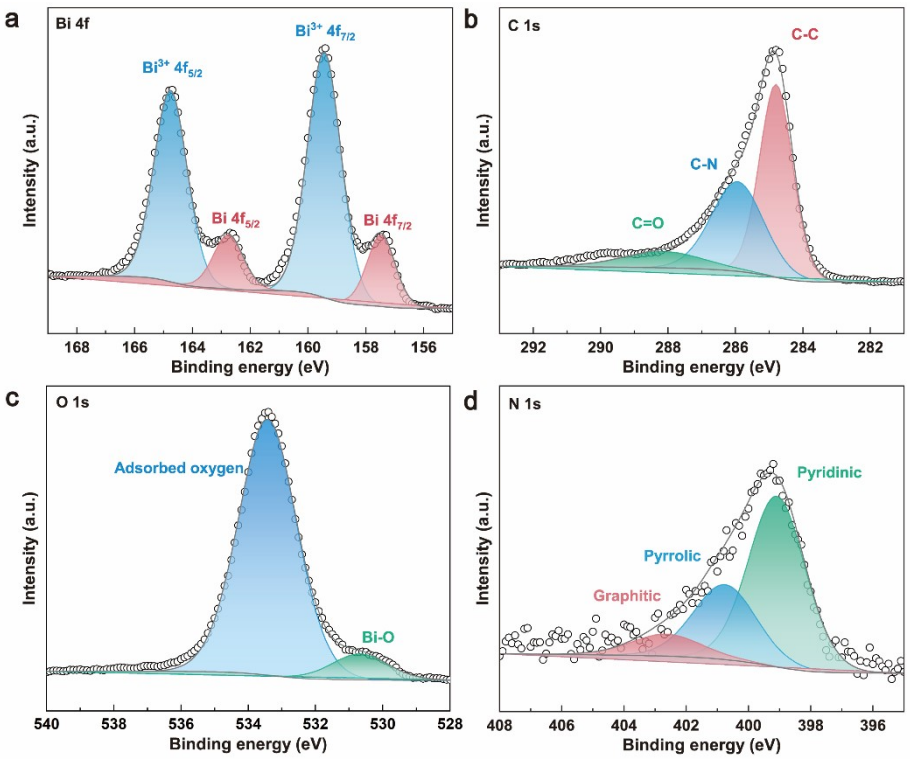

Fig. S4 High-resolution XPS spectra for Bi 4f (a), C 1s (b), O 1s (c) and N 1s (d) of Bi NPs@PG.

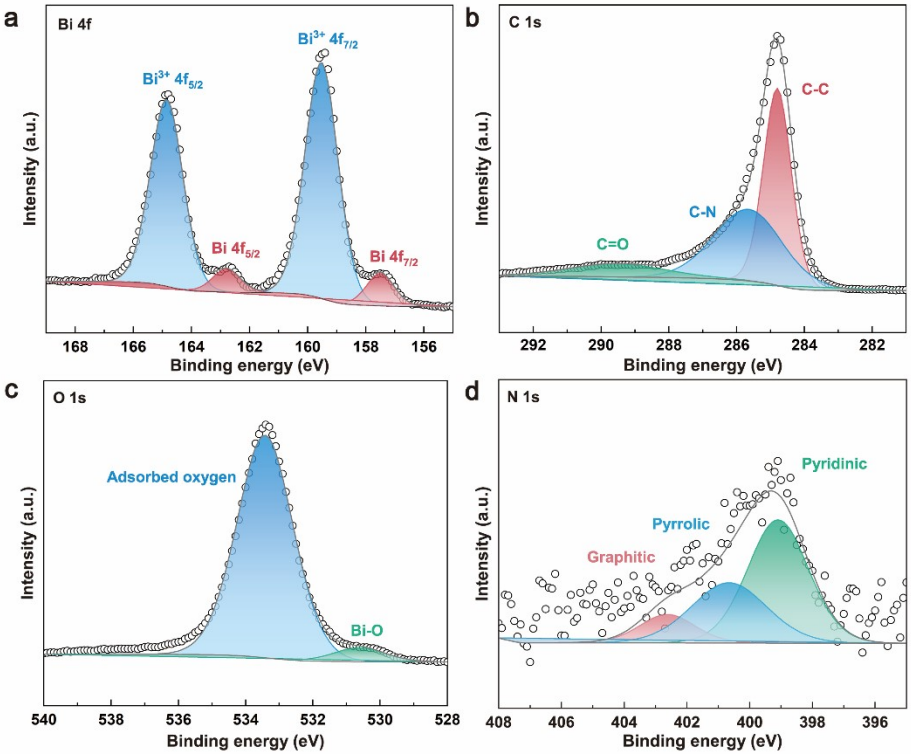

Fig. S5 High-resolution XPS spectra of Bi 4f (a), C 1s (b), O 1s (c) and N 1s (d) for Bi SPs@PG.

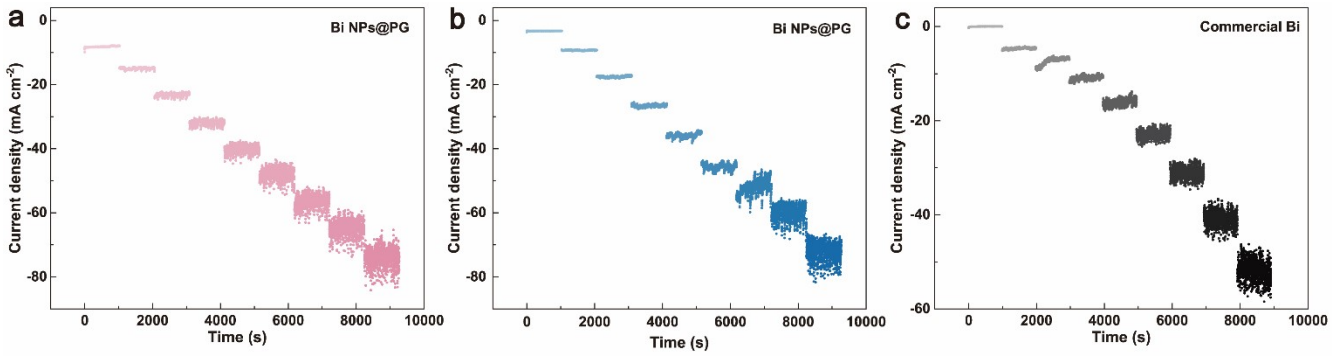

Fig. S6 Typical chronoamperometric curves recorded at potentials ranging from -0.83 V to -1.19 V *vs.* RHE of (a) Bi NPs@PG, (b) Bi SPs@PG and (c) commercial Bi during electrocatalytic CO_2 reduction.

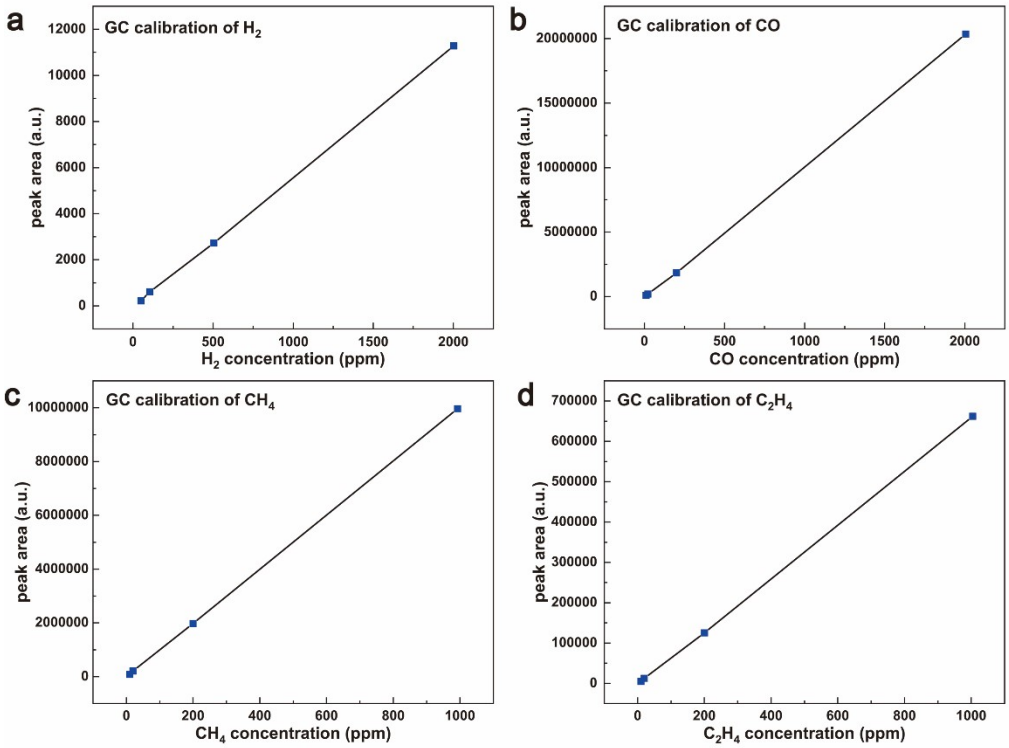

Fig. S7 GC calibration curves for (a) H_2, (b) CO, (c) CH_4, and (d) C_2H_4.

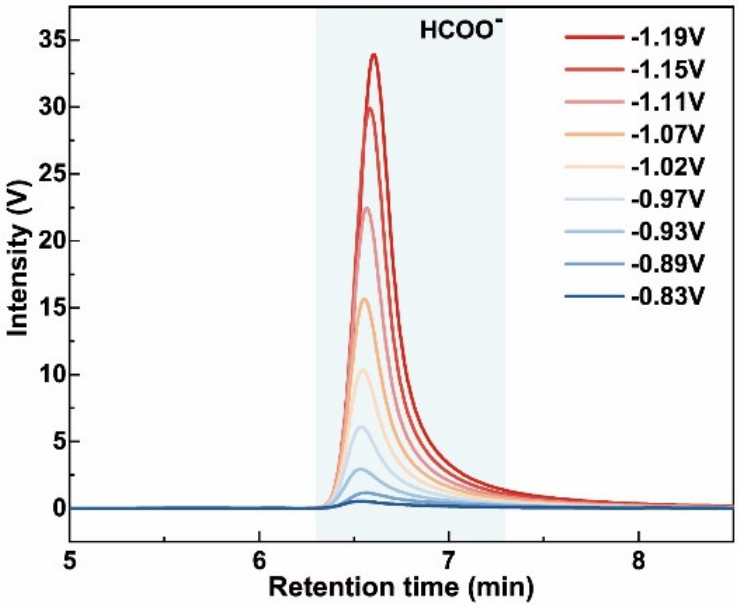

Fig. S8 The ion chromatographic spectra of the liquid product (formate) obtained at various potentials during CO_2RR.

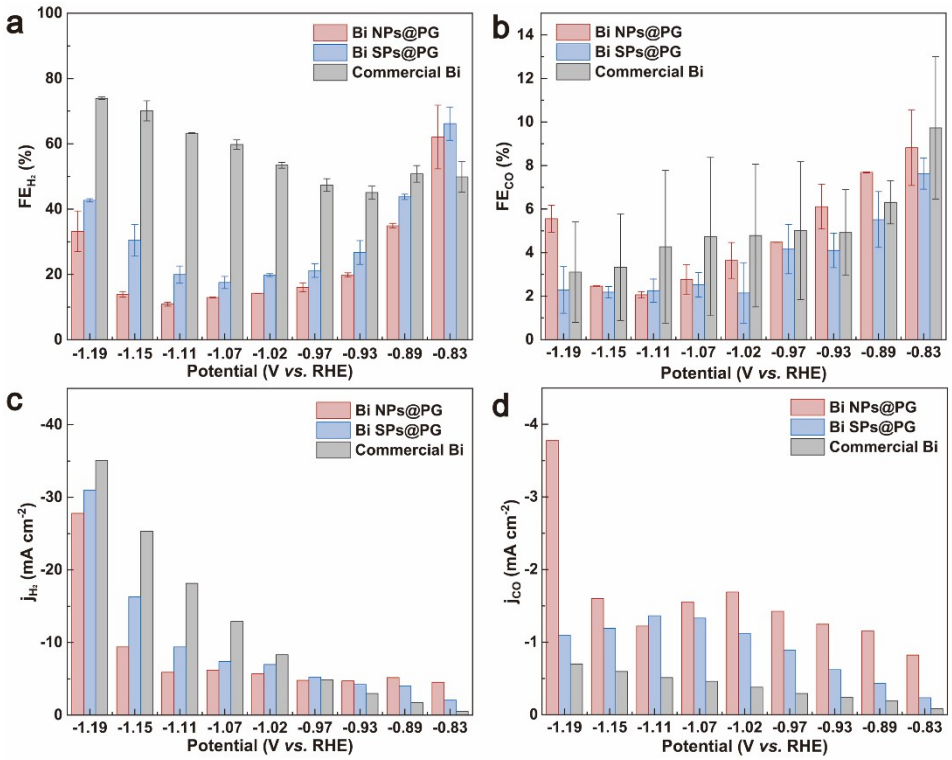

Fig. S9 Comparison of FE for (a) H_2 and (b) CO with the prepared catalysts. The corresponding partial current density for (c) H_2 and (d) CO with the prepared catalysts.

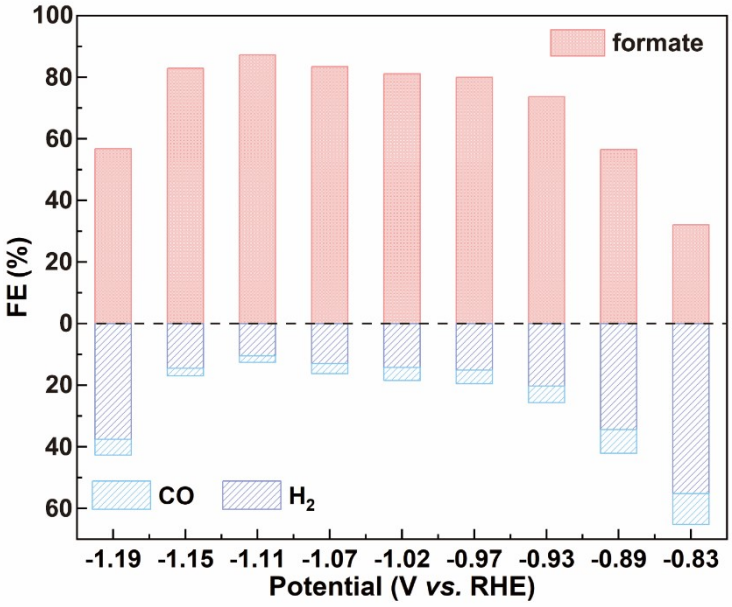

Fig. S10 The total FE of Bi NPs@PG.

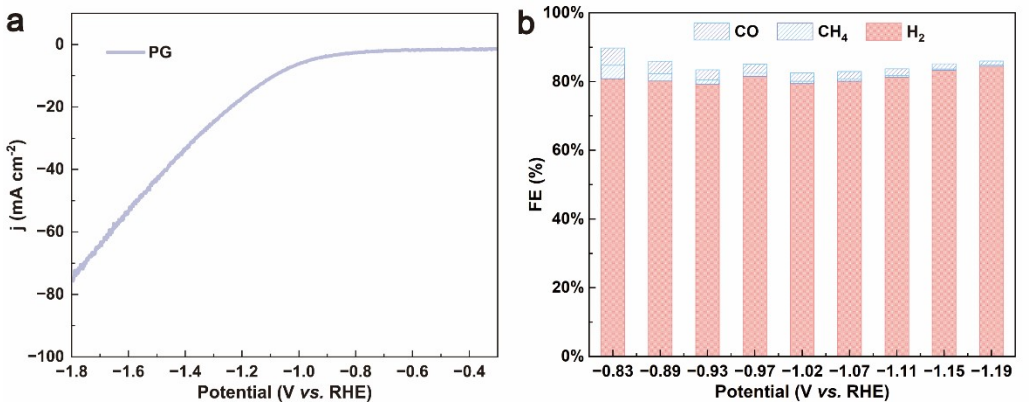

Fig. S11 (a) Linear sweep voltammetry curve and (b) Faradaic efficiency curve of PG catalyst.

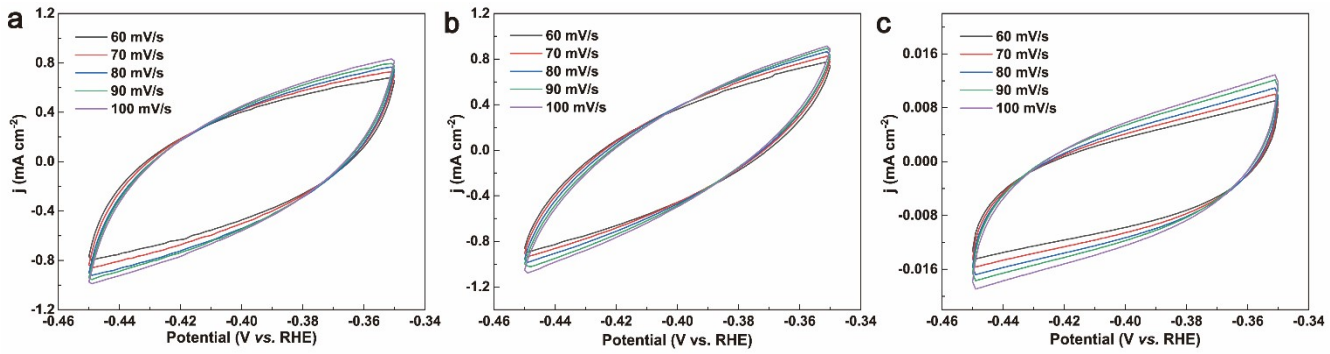

Fig. S12 Cyclic voltammetry curves recorded in the potential range of -0.35 V to -0.45 V *vs.* RHE for (a) Bi NPs@PG, (b) Bi SPs@PG and (c) commercial Bi.

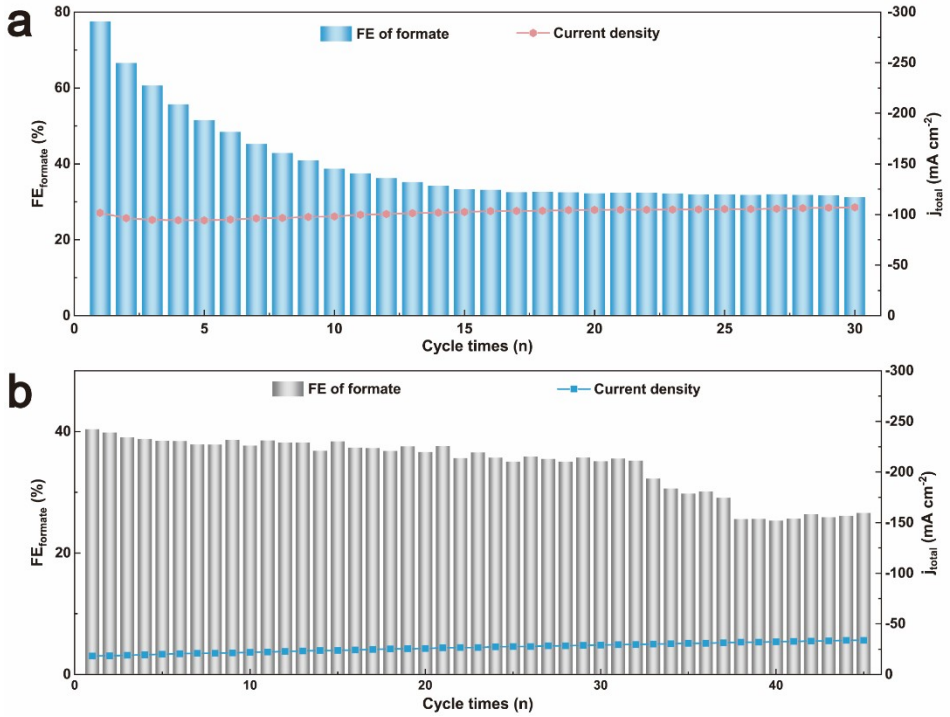

Fig. S13 Long-term stability test for (a) Bi SPs@PG (b) commercial Bi at −1.11 V *vs.* RHE.

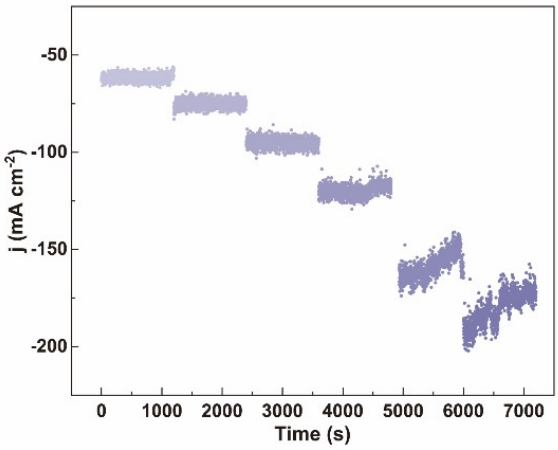

Fig. S14 Typical chronoamperometric curves recorded in a flow cell at potentials ranging from -1.0 V to -1.34 V *vs.* RHE for Bi NPs@PG.

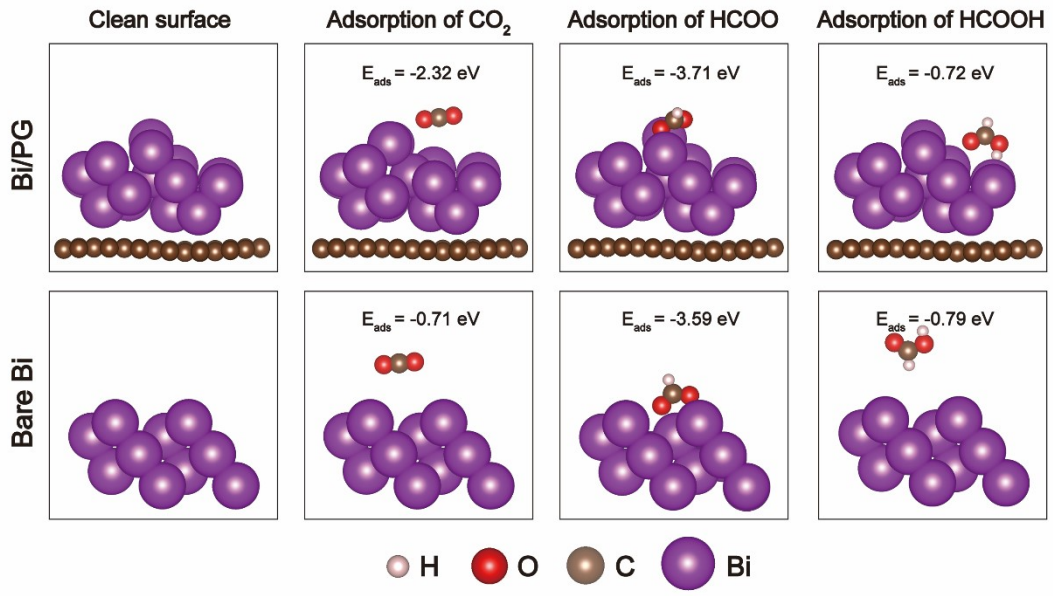

Fig. S15 Side view models of clean surfaces and optimized adsorption configurations of *CO_2, *HCOO and HCOOH on the surfaces of Bi/PG and bare Bi.

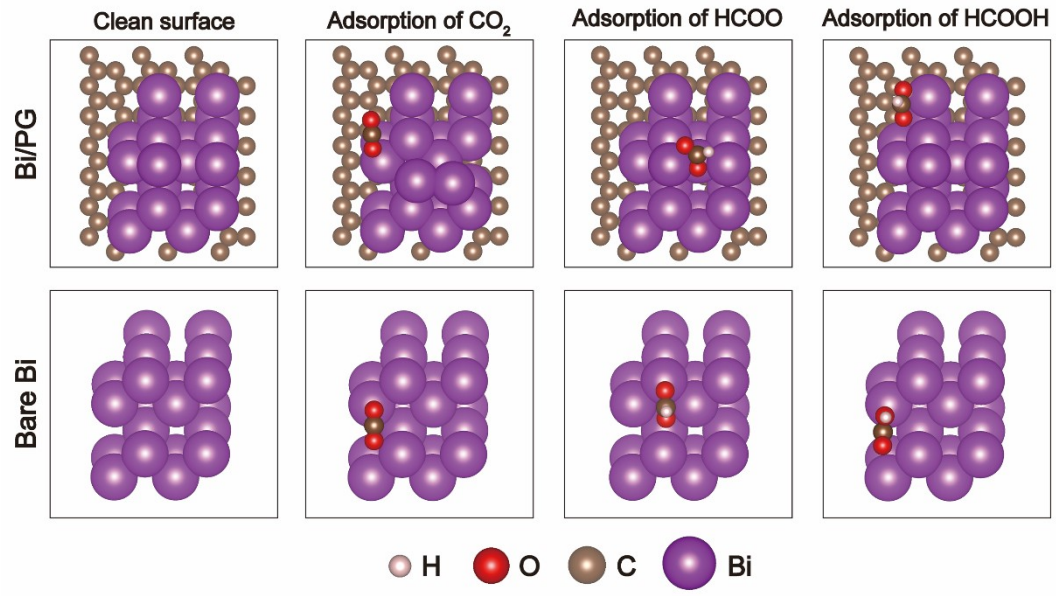

Fig. S16 Top view models of clean surfaces and optimized adsorption configurations of *CO_2, *HCOO and HCOOH on the surfaces of Bi/PG and bare Bi.

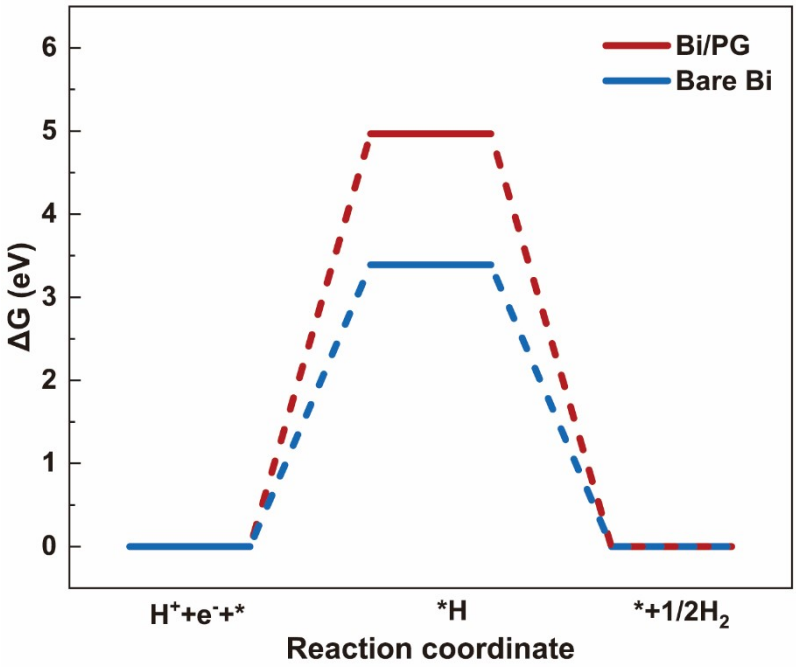

Fig. S17 Calculated Gibbs free energy diagram for hydrogen evolution reaction (HER) on the surfaces of Bi/PG and bare Bi.

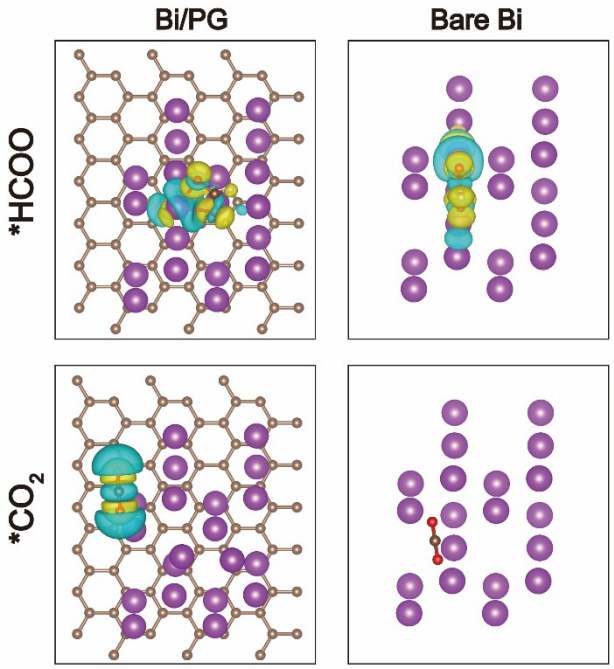

Fig. S18 The top-view charge difference diagrams for the optimized adsorption configurations of *HCOO and *CO_2 on Bi/PG and bare Bi catalysts.

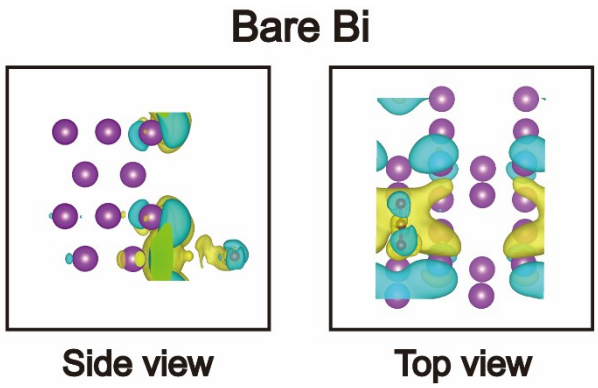

Fig. S19 Side view and top view of charge difference diagrams displaying optimized adsorption configurations of and $*CO_2$ on bare Bi catalyst. The isosurface level set to 0.00002 e $Å^{-3}$, where charge depletion and accumulation were depicted by cyan and yellow, respectively.

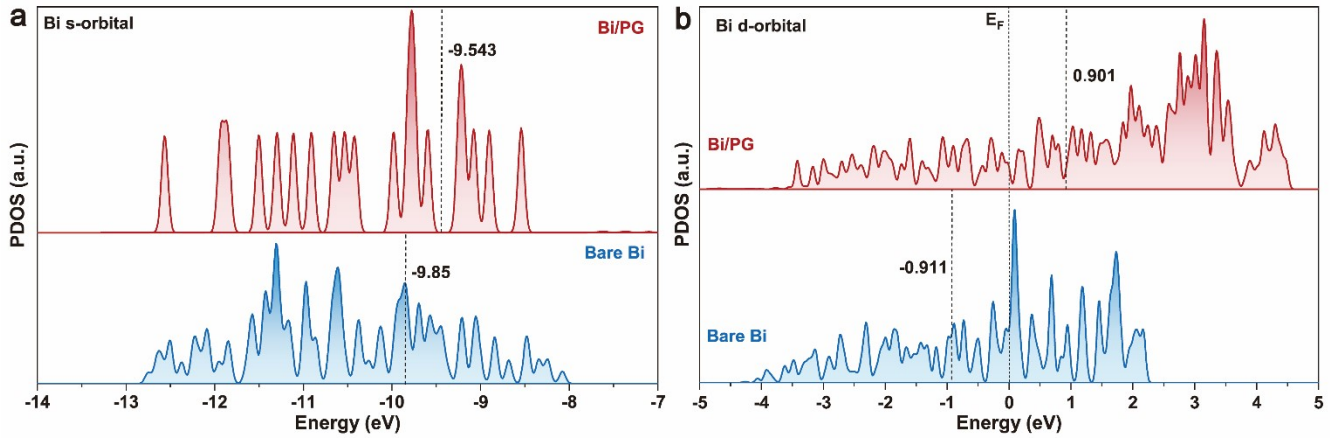

Fig. S20 The projected density of states (PDOS) for (a) s-orbital and (b) d-orbital of Bi in Bi/PG and bare Bi catalysts.

Table S1. DFT total energies (E_{DFT}), zero-point energies (E_{ZPE}), entropies (S) multiplied by temperature (T*S, T=298.15 K), and enthalpies ($\int C_p\, dT$) for the molecules and intermediates on Bi NPs@PG and commercial Bi from DFT calculations.

	E_{DFT} (eV)	E_{ZPE} (eV)	T*S (eV)	$\int C_P dT$ (eV)
H_2	-6.759	0.267	0.403	0.090
CO	-14.436	0.130	0.162	0.090
CO_2	-22.343	0.299	0.664	0.099
Bi/PG	-740.105	-	-	-
*HCOO on Bi/PG	-766.998	0.588	0.204	0.094
*HCOOH on Bi/PG	-770.314	0.885	0.221	0.097
*COOH on Bi/PG	-766.608	0.595	0.186	0.091
*CO on Bi/PG	-754.935	0.139	0.181	0.070
*H on Bi/PG	-739.159	0.144	0.038	0.0227
Bare Bi	-78.119	-	-	-
*HCOO on bare Bi	-105.167	0.592	0.270	0.117
*HCOOH on bare Bi	-108.086	0.894	0.262	0.106
*COOH on bare Bi	-104.491	0.588	0.206	0.096
*CO on bare Bi	-93.077	0.150	0.272	0.109
*H on bare Bi	-78.011	0.140	0.035	0.022

References

1. K. Jiang, R. B. Sandberg, A. J. Akey, X. Liu, D. C. Bell, J. K. Nørskov, K. Chan and H. Wang, *Nature Catal.*, 2018, **1**, 111-119.
2. J. P. Perdew, K. Burke and M. Ernzerhof, *Phys. Rev. Lett*, 1996, **77**, 3865-3868.
3. G. Kresse and J. Furthmuller, *Comput. Mater. Sci.*, 1996, **6**, 15-50.
4. S. Grimme, *J. Comput. Chem.*, 2006, **27**, 1787-1799.
5. G. Kresse and D. Joubert, *Phys. Rev. B*, 1999, **59**, 1758-1775.
6. P. E. Blochl, *Phys. Rev. B*, 1994, **50**, 17953-17979.